



Planetary Boundary Layer variability over New Delhi, India, during EUCAARI project

Konstantina Nakoudi^{1,2}, Elina Giannakaki^{1,3}, Aggeliki Dandou¹, Maria Tombrou¹, Mika Komppula³

5 ¹Department of Environmental Physics and Meteorology, Faculty of Physics, University of Athens, Greece

²Alfred Wegener Institute, Helmholtz Centre for Polar and Marine Research, Potsdam, Germany

³Finnish Meteorological Institute, Kuopio, Finland

Correspondence to: K. Nakoudi (knakoudi@phys.uoa.gr)

10 **Abstract.** Ground-based lidar measurements were performed at Gual Pahari measurement station, approximately 20 km South of New Delhi, India, from March 2008 to March 2009. The height of the Planetary Boundary Layer (PBL) was retrieved with a portable Raman lidar system, utilizing the modified Wavelet Covariance Transform (WCT) method. The lidar derived PBL heights were compared to radiosonde data, Cloud-Aerosol Lidar and Infrared Pathfinder Satellite Observation
15 (CALIPSO) satellite observations and two atmospheric models. The results were also analyzed on a seasonal basis. To examine the difficulties of PBL lidar detection under different meteorological and aerosol load conditions we focused on three case studies of PBL diurnal evolution. In the presence of a multiple aerosol layer structure, the WCT method exhibited high efficiency in PBL height determination. Good agreement with the European Center for Medium-range Weather Forecasts
20 (ECMWF) and the Weather Research and Forecasting (WRF) estimations was found ($r=0.69$ and $r=0.74$, respectively) for a cumulus convection case. In the aforementioned cases, temperature, relative humidity and potential temperature radiosonde profiles were well compared to the respective WRF profiles. The Bulk Richardson Number scheme, which was applied to radiosonde profile data, was in good agreement with lidar data, especially during daytime ($r=0.68$). The overall comparison with
25 CALIPSO satellite observations; namely, CALIOP Level 2 Aerosol Layer Product, was very satisfying ($r=0.84$), with CALIPSO Feature Detection Algorithms slightly overestimating PBL height. Lidar measurements revealed that the maximum PBL height was reached approximately three hours after the solar noon, whilst the daily evolution of the PBL was completed, on average, one hour earlier. The PBL diurnal cycle was also analyzed using ECMWF estimations, which produced a stronger cycle during the winter and pre-monsoon period. The seasonal analysis of lidar PBL heights yielded a less pronounced PBL cycle than the one expected from long term climate records. The lowest mean daytime PBL height (695 m) appeared in winter, while the highest mean daytime PBL height (1326 m) was found in the monsoon season as expected. PBL daily growth rates exhibited also a weak seasonal variability.

35 **1 Introduction**

The Planetary Boundary Layer (PBL) is the lowermost portion of the troposphere, which experiences a diurnal cycle of temperature, humidity, wind and pollution variations. The PBL height is required in



numerous applications; for instance, in pollution-dispersion modeling, where the upper boundary of the turbulent layer plays a role as an impenetrable lid for pollutants released at the surface. PBL height also appears as a mixing scale height in turbulence closure schemes within climate and weather prediction models (Zilitinkevich and Baklanov, 2001). As air pollution becomes more severe due to economic development, particularly in developing countries (Wang et al., 2009), observations of the PBL height with high temporal and vertical resolution are essential for weather and air-quality research. Moreover, PBL height is related to the warming rate caused by enhanced greenhouse gases emissions (Pielke et al., 2007).

Several methods have been proposed to estimate PBL height, utilizing vertically resolved thermodynamic variables, turbulence-related parameters and concentrations of tracers (Seibert et al., 2000; Emeis et al., 2004). Lidar (Light Detection And Ranging) systems can provide continuous measurements of various atmospheric quantities, including the vertical distribution of atmospheric aerosols from which the PBL height can also be retrieved (Menuet et al., 1999; Cohn and Angevine, 2000; Brooks 2003; Amiridis et al., 2007; Morille et al., 2007; Baars et al., 2008; Engelmann et al., 2008; Groß et al., 2011; Tsaknakis et al., 2011; Haeffelin et al., 2012; Cimini et al., 2013; Scarino et al., 2013; Summa et al., 2013; Korhonen et al., 2014; Lange et al., 2014; Bravo-Aranda et al., 2016; de Arruda Moreira et al., 2018). Atmospheric aerosols are used as tracers and the PBL top is indicated by a gradient in the range-corrected lidar signal.

New Delhi is one of the most densely populated cities, with 29259 inhabitants per square mile, and the fifth most populous city in the world according to United Nations population estimates and projections of major Urban Agglomerations (<https://esa.un.org/unpd/wup/>), with an estimated 2016 population of 18.6 million. It is surrounded by the Thar Desert to the west and the western Indo-Gangetic Plain to the north. Particulate air pollution in this area is assumed to originate from fossil fuel and biomass burning besides natural sources such as desert dust (Hedge et al., 2007; Ramanathan et al., 2007a). The identification of the layer height within which pollutants are trapped is particularly important in this polluted area, since the largest and most persistent pollution haze covers an area of about 10 million km² over Southern Asia (Nakajima et al., 2007; Ramanathan et al., 2007a). Thus, vertically resolved observations are indispensable to reveal information regarding local air quality, climate change and human health related issues.

Despite the importance of the area under investigation, only few ground-based measurements of aerosol vertical profiles have been carried out, with most of the available data accessed during short field campaigns (Lelieveld et al., 2001; Nakajima et al., 2007; Ramanathan et al., 2007a). In this study, we investigate PBL characteristics over New Delhi, India, based on one year long ground-based lidar measurements. The measurements were carried out from March 2008 to March 2009 in the framework of EUCAARI (European Integrated project on Aerosol Cloud Climate and Air Quality Interactions) project (Kulmala et al., 2011).

The aim of this paper is twofold; (1) to retrieve and statistically analyze the PBL height, derived from ground-based lidar measurements and (2) to compare it to heights from independent data sources. The auxiliary sources comprised radiosonde data, space-borne lidar observations and simulations from two atmospheric models.



2 Measurement site

The lidar measurement site was located at Gual Pahari (28.43°N, 77.15°E, 243 m A.S.L.), which is
80 situated in the Gurgaon district of Haryana state, about 20 km south of New Delhi, India (Hyvärinen et
al., 2010; Komppula et al., 2012). The surroundings of the station represent a semi-urban environment
with agricultural test fields and light vegetation. There were no major pollution sources, except for the
road between Gurgaon and Faridabad about 0.5 km to the south-west of the station, while only electric-
powered vehicles were allowed at the station area. Anthropogenic sources in the greater region
85 comprised traffic, city emissions and power production (Reddy and Venkataraman, 2002a, b).

Meteorological quantities were measured at the meteorological station of Safdarjung airport (28.58°N,
77.21°E, 211 A.S.L.), New Delhi, which is located 18 km NW of Gual Pahari and was the closest
climatological site to the lidar measurement site.

During the measurement period, sunrise time varied between 5:45 and 7:15 LST, whilst sunset
90 appeared between 18:15 and 19:15 LST. Solar noon appeared between 12:00 and 12:30 LST. Local
time at New Delhi corresponds to UTC+5.5 h. From now on in this paper, UTC will be adopted, since
the synchronization of results from lidar measurements and numerical simulations would have been
difficult, if the LST convention was used.

In 2008, the highest temperature was recorded in May, with a monthly maximum temperature of 36.9
95 °C. The annual mean temperature was 24.6 °C in 2008 and 25.4 °C in 2009. Monthly maximum
temperatures during May and June were 3 to 4 °C lower than the climatological values (World
Meteorological Organization, <http://worldweather.wmo.int/en/city.html?cityId=224>), while February
and March (temperature average of March 2008 and March 2009) were characterized by almost 3 °C
higher maximum temperatures, as shown in Figure 1(a). The year 2008 exhibited the most rainfall,
100 between June and September, compared to the four year period 2006-2009, with a total of 570 mm in
Gual Pahari (Hyvärinen et al., 2010). However, rainfall (June-September) was lower than the
climatological value of 602 mm in New Delhi. In the monthly periods from April to June and August to
September 2008, the total precipitation was higher than the one expected from climatology, with a
maximum anomaly appearing in May, whereas in July 2008 cumulative precipitation was lower (Figure
105 1(b)). This year also exhibited an early monsoon onset date on 16 June, which was one of the earliest
onset dates recorded in the area with rainfall data available since 1901 (Tyagi et al., 2009). The Indian
summer monsoon in 2008 was somewhat weaker than normal, following the La Niña condition in the
tropical Pacific (Lau et al., 2009).

3 Methods

3.1 Ground-based lidar measurements

3.1.1 FMI-Polly^{XT} lidar system

The measurements were conducted with a six channel Raman lidar called FMI-Polly^{XT} (Finnish
115 Meteorological Institute - Portable Lidar sYstem eXTended). The lidar system was entirely remotely
controlled via an internet connection, with all the measurements, data transfer and built-in device
regulation being performed automatically. The instrument was equipped with an uninterruptible power



supply (UPS) and an air conditioning system (A/C) to allow for safe and smooth continuous measurements. A rain sensor was also connected to the roof cover in order to assure a proper shutdown of the instrument during rain.

120 FMI-Polly^{XT} lidar used a Continuum Inline III type laser. The pulse rate of the laser was 20 Hz and it delivered energies of 180, 110 and 60 mJ simultaneously (with external second and third harmonic generators) at three different wavelengths, i.e. 1064, 532, 355 nm, respectively. The vertical resolution of the system was 30 m and the vertical range covered the whole troposphere under cloudless conditions. The output of the instrument included vertical profiles of the particle backscatter coefficient at three wavelengths, i.e. 355, 532 and 1064 nm, extinction coefficient at 355 and 532 nm and linear
125 particle depolarization ratio at 355 nm. The FMI-Polly^{XT} lidar system is described in more detail in Althausen et al. (2009) and Engelmann et al. (2016). Table 1 presents the relevant properties of FMI-Polly^{XT}, together with the properties of the other techniques utilized. The other techniques will be discussed in the following Sections.

3.1.2 PBL top detection technique

130 The PBL height was derived from the 15 min averaged lidar backscatter signals at 1064 nm using the wavelet covariance transform (WCT) method (Brooks, 2003) with modifications introduced by Baars et al. (2008). The WCT method makes use of the assumption that the PBL contains much more aerosol load compared to the free troposphere and, thus, a strong backscatter signal decrease can be observed at the PBL top. The covariance transform $W_r(a,b)$ is a measure of the similarity between the range-
135 corrected lidar signal and the related Haar function (Baars et al., 2008). This method was chosen because it allows larger adjustability than other techniques, as shown from previous studies (Baars et al., 2008; Korhonen et al., 2014). For instance, the gradient technique involves an ambiguity in the choice of the “relevant” minimum in the gradient that corresponds to the boundary layer height (Lammert and Bösenberg, 2005).

140 A threshold value of the WCT which permits the identification of a significant gradient and the omission of weak gradients was introduced as a first modification. The first height above ground at which a local maximum of $W_r(a,b)$ occurred, exceeding a signal decrease threshold, was defined as the PBL height. This threshold was modified in cases of multiple aerosol layers structures, where strong gradients inside the PBL complicated the detection of the PBL height. Furthermore, the option to cut
145 the lower parts of the signal (from 30 to 870 m) was utilized so as to avoid strong gradients related to the incomplete overlap in the lower heights. The importance of a proper threshold adjustment is discussed in Section 4.1, where three case studies are analyzed and the applicability of the WCT method, under different meteorological and aerosol load conditions, is examined.

The WCT method also allows for the detection of clouds by means of a negative threshold. Baars et al.
150 (2008) found that cloud screening works well for a threshold of -0.1. The cloud base is given one height bin below the altitude at which $W_r(a,b)$ is lower than the chosen threshold value.

The incomplete overlap between the laser beam and the receiver field of view (L-R) (Wandinger and Ansmann, 2002) restricts the observational detection range to heights above 200-300 m. This is partly counterbalanced by the overlap correction function, which was calculated at 532 nm. During the



155 measurement campaign, the L-R overlap was complete at 550-850 m. However, PBL detection can be made reliably down to 200-300 m, because the increasing overlap with height causes an increasing signal with height. Hence, the detection of the convective Boundary layer (CBL) is not disturbed, since the CBL is usually higher than 300 m (Korhonen et al., 2014). During night-time, the configuration of FMI-Polly^{XT} permitted the detection of the residual layer (RL).

160 Daily mean and maximum PBL heights correspond to convective hours (3:00-12:00 UTC). The hourly PBL height values were calculated from the 15 min lidar data by averaging of the three closest data points of the time considered (e.g. 12:00 hourly height would be the average of the three data points between 11:45 and 12:15). The seasonal cycle study was based on the classification proposed by the Indian Meteorological Department, i.e. winter (December-March), pre-monsoon or summer (April-
165 June), monsoon (July-September) and post-monsoon (October-November) (Perrino et al., 2011). However, the PBL seasonal cycle was examined during the winter, pre-monsoon and monsoon periods, as no sufficient data coverage was found during the post-monsoon period. The diurnal PBL cycle is provided by lidar measurements and ECMWF estimations for the whole measurement period as well as on a seasonal basis (Section 4.3.1).

170 The PBL growth period was determined following the guidelines of Baars et al. (2008). More specifically, the PBL growth period began when the PBL height started to increase (typically 2-4 h after sunrise) and was completed when 90% of the daily maximum height was reached (typically between 08:00 and 10:30 UTC). Regarding the daily evolution rate, this was determined through the slope of a linear fit to the hourly height values (between the start and the completion of the growth
175 period). Furthermore, the calculation of the evolution rate was restricted to cases where at least 4 consecutive or 3 non- consecutive hourly values were available. Due to these restrictions, the evolution rate was determined for 51 days.

3.1.3 Data coverage

180 During the one year long measurement campaign, from 12 March 2008 to 31 March 2009, FMI-Polly^{XT} was measuring on 139 days. Due to technical problems with the laser (27%), the data coverage from September to January was sparse. Furthermore, precipitation prohibited lidar measurements, since the lidar system had to shut down (12%). Thus, lidar measurements were possible in 61% of the total time (139 days).

185 Sufficient data availability (more than 25%, from 4 h after sunrise to 1 h before sunset) was achieved during 72 days. During these days, multiple aerosol layer structures (20%) and low clouds (15%) complicated PBL height detection. Additionally, some technical issues arose due to photomultiplier supersaturation and signal problems (9%). A lack of a significant decrease in the backscatter profile was observed in only a few cases (3%). The latter was a first indication that the modified WCT method could detect the PBL top efficiently, as long as the signal decrease threshold was tuned properly.

190 Hence, the PBL height could be identified in 53% of the cases with sufficient data availability (72 days). In Figure 2, the data coverage is presented on a monthly basis. The highest PBL detection frequency was achieved in February, reaching 74%. This high detection rate can be attributed to



favorable meteorological conditions, since in February the occurrence of low clouds was 0.7% with no rainfall events.

195 3.2 Radiosonde measurements

Radiosondes have been routinely used for decades and therefore are a valuable method for long term climatology analyses (Seidel et al, 2010; Wang and Wang, 2014). Restrictions of radiosondes refer to the coarse vertical resolution of standard meteorological data with respect to boundary layer studies as well as the smoothing due to the sensor lag constant bounded by the high ascent rate of the radiosonde (Seibert et al., 2000). In this study, the main restriction is that radiosonde and lidar measurements were not collocated, since radiosonde data from the meteorological station of Safdarjung airport (18 km from the lidar site) were used. The radiosonde data were obtained from the University of Wyoming (<http://weather.uwyo.edu/upperair/sounding.html>) for the station number VIDD 42182. Radiosondes were launched on a regular basis, twice a day at fixed times, 00:00 UTC and 12:00 UTC.

205 The Bulk Richardson Number (BRN) method was used for PBL determination, employing the formula introduced by Menut et al. (1999):

$$Ri_b(h) = \frac{g(h-h_0)}{\theta(h)} \frac{[\theta(h) - \theta(h_0)]}{u(h)^2 + v(h)^2}$$

, where h is altitude, h_0 the altitude of the ground, g gravitational acceleration, θ potential temperature in Kelvin and u and v the zonal and meridional wind components, respectively. The PBL height was determined to be the lowest altitude where BRN reached the critical value, which is taken equal to 0.21 (Vogelezang 1996). Beyond this critical value of R_i , the atmosphere can be considered stable and fully decoupled from the underneath layer.

215 3.3 Space-borne lidar observations

Cloud-Aerosol Lidar and Infrared Pathfinder Satellite Observation (CALIPSO) is an Earth Science observation mission that was launched on 28 April 2006. The vertical resolution of the CALIOP (Cloud-Aerosol Lidar with Orthogonal Polarization) system is 30 m. CALIPSO Level 2 aerosol layer product provides a description of the aerosol layers, including their top and bottom height, identified by automated algorithms applied in the Level 1 data. Detailed description of the aforementioned algorithms can be found in Vaughan et al. (2004) and Winker (2006). Currently, no operational CALIOP PBL product is available.

In this study, we use CALIOP Level 2 Aerosol Layer Product, which provides information on the base and top heights of existing aerosol layers, reported at a uniform 5 km horizontal resolution. Leventidou et al. (2013) evaluated the PBL height derived by Level 2 Aerosol Layer products over Thessaloniki, Greece, for a 5 year period, making the assumption that the lowest aerosol layer top can be considered as the PBL height. The aforementioned method was also applied over South Africa, revealing high agreement with ground based observations (Kohronen et al., 2013). During the measurement campaign, the PBL height was also accessed by the space-borne lidar CALIOP, within two overpass distances, 20 and 101 km from Gual Pahari.

230



3.4 Atmospheric model estimations

3.4.1 The ECMWF model

The ECMWF (European Center for Medium-range Weather Forecasts) runs a global weather forecast model as part of an integrated forecast system. We have used a global model grid with 1.0 ° horizontal resolution and 62 vertical pressure levels from ground up to 5 hPa. The total time of each model run was 240 h, while the temporal resolution was 3 h for the first 72 h and 6 h after this initial period (ECMWF, 2010a, b). A more detailed description of the model is given in ECMWF (2010c). In the present study, only the PBL height model parameter was used. The PBL height for the lidar site in Gual Pahari was found by interpolation using inverse-distance weighted averages of the four closest grid points, at distances of 96, 50, 104 and 65 km.

The ECMWF model defines the PBL height by using the BRN method with R_{icr} value of 0.25 (ECMWF, 2010b). The atmospheric turbulence is determined based on local stability. In unstable local conditions ($R_i < 0$), the exchange coefficients are based on local similarity (Nieuwstadt, 1984). In stable local conditions ($R_i > 0$) enhanced diffusion coefficients according to the Louis, Tiedtke, Gleyne scheme (Louis et al., 1982), revised by Beljaars (1995), Beljaars and Viterbo (1999) and Viterbo et al. (1999) are used close to the surface. ECMWF output data were used in the PBL heights comparison in three case studies that are analyzed in Section 4.1, as well as in the examination of the mean diurnal PBL Cycle (Section 4.3.1).

3.4.2 The WRF model

The WRF model, Version 3.9.1 (Skamarock et al., 2008) was also applied in order to determine the PBL height. The simulation domain was centered at the lidar station in Gual Pahari and three domains with a respective horizontal resolution of 18 km, 6 km and 2 km were used, where the two inner domains are two-way nested to their parent domain. The third inner-most domain covers an area between 75.84-78.46° E and 27.38-29.52° N. The output is provided every hour. On the vertical axis, 37 full sigma levels resolve the atmosphere up to 50 hPa (≈ 20 km AGL), with a finer grid spacing near the surface. In this study, the Yonsei University scheme (YSU) (Hong et al., 2006) in conjunction with the land surface model Noah (Chen and Dundhia, 2001) was used for the estimation of PBL height. In addition, the Rapid Radiative Transfer Model (RRTM) scheme (Mlawer et al., 1997) for longwave radiation and the scheme of Dundhia (1989) for shortwave radiation were applied. A surface-layer scheme based on the revised MM5 similarity theory (Jimenez et al., 2012) as well as the Kain and Fritsch (1990, 1993) scheme for cumulus parameterization were used. For microphysics, the scheme proposed by Thompson et al. (2008) was considered. Regarding land use and soil types, the predefined datasets of Moderate Resolution Imaging Spectroradiometer (MODIS) with 21 land use classes were used. The initial and lateral boundary conditions were derived from the National Center for Environmental Prediction (NCEP) operational Global Fine Analysis (GFS) with 1 ° x 1 ° spatial resolution and were updated every 6 h. The Sea Surface Temperature (SST) was obtained from High Resolution Real-Time Global SST (RTG SST HR), with spatial resolution 0.083 ° x 0.083 ° which was renewed every 24 h.



270 In the YSU scheme, the top of the PBL height under unstable conditions is determined as the first
neutral level based on the BRN calculated between the lowest model level and the levels above (Hong
et al., 2006; Shin and Hong, 2011). Under stable conditions, the BRN is set as a constant value of 0.25
over land, enhancing mixing in the stable boundary layer (Hong and Kim 2008), whereas it is a
function of the surface Rossby number over the oceans, following the study of Vickers and Mahrt
(2003).

275 Within the frame of three case studies, the default simulated PBL height from WRF was used to justify
the lidar PBL heights. Furthermore, WRF profiles of temperature (T), relative humidity (RH) and
potential temperature (θ) were compared to corresponding radiosonde profiles. The comparison was
performed through specific criteria following the guidelines given by Seidel et al. (2010). In the T
280 criterion, the base of an elevated temperature inversion is considered as the PBL top. Inversions do not
appear in every profile, but when present, their base serves as a cap to the mixing processes below. In θ
profiles, the level of the maximum vertical gradient (Oke, 1988; Stull, 1988; Sorbjan 1989; Garrat,
1992) was used, since this gradient is indicative of a transition from a convectively less stable region
below to a more stable region above. In a similar way, the level where an abrupt reduction of RH
appears is considered as the PBL top.

285 **4 Results and discussion**

4.1 Applicability of the WCT method: Case studies

Three case studies of PBL daily evolution were analyzed and evaluation with ancillary data sources
was performed so as to investigate their strengths and limits. First, the evolution of PBL under
cloudless conditions is discussed for 12 February 2009. Subsequently, a two-day case with a multiple
290 aerosol layer structure is presented for 1-2 March 2009. Finally, the diurnal development of PBL is
investigated in the presence of low clouds for 29 June 2008. The three criteria (T_{crit} , RH_{crit} , θ_{crit})
were used to determine PBL height in each radiosonde profile. These criteria were also applied to WRF
data. The results from the utilized methods are presented in Tables 2 and 3 for the night-time and
daytime period, respectively.

295 It was found that the presence of multiple aerosol layers and low clouds can pose difficulties in PBL
top detection (Section 3.1.3). However, as it will be shown these difficulties can be dealt with the use
of proper WCT threshold and cut off values (see Section 3.1.2).

4.1.1 Cloud free case: 12 February 2009

300 The diurnal evolution of PBL during 12 February 2009 is presented in Figure 3. Sunrise was
approximately at 01:30 UTC, while sunset was at 12:40 UTC. No aerosol layers were found aloft.
Between 06:00-12:00 UTC, although internal gradients (yellow and red color) of aerosol content
appeared inside the PBL, the default signal decrease threshold (0.05) was efficient. Between 12:00-
18:00 UTC a threshold of 0.08 was used in conjunction with a 90 m cut-off height. Due to low aerosol
load content, the derived PBL heights between 12:00-14:00 UTC showed high variability. An almost
305 constant daily growth rate of 133 m/h was found from 06:00 UTC to 10:00 UTC. The maximum height
of 950 m was reached at 10:30 UTC.



Figure 3 (middle panel) shows the development of PBL according to FMI-Polly^{XT} measurements and the estimations from the two atmospheric models. During convective hours (05:00-12:00 UTC), the WRF and ECMWF models seemed to overestimate PBL height. On the other hand, during night-time model estimations yielded lower PBL heights compared to lidar data, since the former estimated the nocturnal PBL while the latter identified the RL top. Between 6:00 and 12:00 UTC, FMI-Polly^{XT} identified a light aerosol load activity at the altitude where the WRF model estimated the PBL height. The correlation with lidar hourly heights was satisfying ($r=0.8$) for both model output data, while a mean normalized bias of 11% and 16% was found for WRF and ECMWF data, respectively.

310 During night-time, radiosonde profiles determined PBL height at 435 m (θ_{crit} and RH_{crit} methods), while PBL heights of 172 (T_{crit}) and 131 m (θ_{crit} and RH_{crit} methods) were given by WRF data (Table 2). During daytime, the T_{crit} and θ_{crit} methods yielded PBL heights at 1425 m and 1387 m when applied to WRF and radiosonde data, respectively (Table 3). The RH_{crit} revealed slightly lower values at 1213 m (WRF) and 1069 m (radiosonde).

315

320 Regarding the Top of 1st Layer (398 m) as derived from CALIOP Level 2 data, it appeared to well agree with the respective PBL height from FMI-Polly^{XT} (472 m), with a relative difference of 16%.

4.1.2 Case with multiple aerosol layers: 1-2 March 2009

During the two day period of 1-2 March 2009, a complex aerosol layer structure appeared up to 3 km altitude (Figure 4). However, the modified WCT method managed to detect the top of the PBL in most of the 15 min intervals, after modifying the signal decrease threshold and applying a cut-off height. The threshold was adjusted within the range of 0.03-0.08, which corresponds to a 6-16% signal decrease, respectively. Furthermore, a 30-60 m cut-off height was used, in order to avoid gradients in the lower parts of the PBL.

325

330 On 1 March 2009, the transition period (02:00 to 05:00 UTC) was characterized by a slow PBL development of 14 m/h, whereas the PBL evolution was more pronounced in the convective period (05:00 to 09:00 UTC) with a mean growth rate of 101 m/h. The maximum height of 950 m appeared at 08:45 UTC. On the next day, a stronger but slightly shorter PBL cycle was observed, with a mean evolution rate of 187 m/h, reaching a maximum height of 1010 m at 08:15UTC. This slight modification in the development of the PBL, can be attributed to the combination of higher temperature and lower wind speed conditions characterizing the second day.

Output data from ECMWF model, overestimated PBL heights during convective hours (6:00-12:00 UTC), whereas during night-time an underestimation of PBL heights was observed. Nevertheless, the correlation of PBL heights between FMI-Polly^{XT} and ECMWF was very satisfactory for both days ($r=0.99$ and $r=0.92$ on 1st and 2nd of March, respectively). Furthermore, the mean normalized bias values were found 23.4% and 32.6% during the first and second day, respectively.

340

On the first day, WRF output data overestimated PBL height during the transition period from CBL to RL (11:00-14:00 UTC), while on the second day an overestimation was observed during convective hours (9:00-12:00 UTC). On both days, WRF model data underestimated PBL height during the early morning and night hours. Correlation coefficients of 0.92 and 0.95, whilst mean normalized bias values of 15.6% and 37.2 % were found on 1 and 2 March, respectively.

345



In the night-time of 1 March no criteria could be applied to radiosonde data due to sparse vertical resolution (Figure 4). Thus, no comparison could be carried out with WRF heights. In the daytime, radiosonde profiles revealed slightly lower PBL height (582 m) compared to the one given from WRF data (716 m) according to the θ_{crit} and RH_{crit} methods (Table 3). On the 2 March, radiosonde profiles overestimated the night-time PBL height according to all of the three methods, whereas in the daytime the WRF profile of RH yielded a significantly higher PBL height compared to the corresponding radiosonde profile (PBL height at 906 m and 544 m, respectively).

4.1.3 Case with low clouds: 29 June 2008

During this day, the strongest PBL evolution was observed between 3:00 and 5:00 UTC, where the PBL height increased by approximately 553 m/h. On average, a moderate PBL evolution rate of roughly 86 m/h was found, with a maximum height of 1279 m appearing at 9:15 UTC (Figure 5).

In this case broken cumulus clouds appeared between 600-1100 m from 00:00 to 12:00 UTC. The assumption that cloud base constitutes an approximation of the PBL top was made. However, it could be argued that the PBL top was located at a higher level, since diffuse aerosol layers were also present there. During this period, it was difficult to locate an adequate signal decrease gradient; a threshold corresponding to 10% decrease was used, while sensitivity tests with lower threshold values yielded the same results. Hence, the algorithm-decreased sensitivity is mainly related to the diffuse aerosol layers.

Large PBL height values also appeared around 12:00 UTC, corresponding to a strong aerosol layer which sprawled to lower heights, probably due to dry removal or precipitation that evaporated before reaching the ground. Rainfall was observed between 13:30 and 14:30 UTC. After the rainfall period the remaining aerosols kept being displaced in the downward direction, creating strong gradients below 500 m. The effect of aerosol removal can be seen between 16:00 and 24:00 UTC, where low aerosol load conditions are easily observed in the 300-1000 m altitude range. Once again, the low aerosol load observed, complicated the detection of the PBL top by the algorithm and was, thus, responsible for the high variation in the detected PBL heights between 16:00 and 24:00 UTC.

WRF and ECMWF estimations correlated well with FMI-Polly^{XT} hourly PBL height data ($r=0.74$ and $r=0.69$, respectively). During daytime, WRF slightly overestimated PBL height, while an underestimation was observed during night-time by both models. Good agreement was corroborated by additional statistical parameters. Fractional bias was equal to 0.015 and 0.11 for WRF and ECMWF estimations, respectively.

The profile criteria yielded slightly lower PBL heights when applied to the radiosonde profiles during night-time (PBL height at 833 m and 913 m from radiosonde and WRF, respectively) (Table 2). The T_{crit} method revealed the same PBL height (913 m) with the other two methods when applied to WRF data in the night-time. During daytime, the same PBL height (1490 m) was revealed according to the θ_{crit} and RH_{crit} methods from both radiosonde and WRF data (Table 3).

4.2 Comparison of lidar PBL heights to ancillary data sources

4.2.1 Comparison with radiosonde data



PBL heights from FMI-Polly^{XT} were compared to heights from radiosonde profile data. The
385 comparison was performed both during daytime and night-time.

The evaluation of PBL heights during daytime (Figure 6) revealed very satisfying agreement, with an r
of 0.68 ($N=31$). The slope of the fit was 0.95 (y intercept set to zero in all fittings), with radiosonde
PBL heights being lower than lidar PBL heights in 58% of the cases.

390 During night-time ($N=27$) a lower r of 0.47 was found and a slope of 0.36. A systematic source of
deviation was introduced due to the technical setup of the lidar system. More specifically, the
incomplete L-R overlap prohibited the detection of layers lower than 200 m and consequently the
detection of nocturnal PBL height. An additional discrepancy source was the distance between the lidar
station and the radiosonde launch site. We investigated whether the lidar-radiosonde comparison was
affected by wind speed and wind direction, without finding any noticeable correlation. Another
395 deviation source was the much lower vertical resolution of radiosonde profile data in comparison to
vertical profiles of lidar data. Furthermore, the two methods are inherently different. The WCT method
uses the vertical distribution of aerosols as a tracer, whereas the BRN method is based on profiles of
thermodynamic and dynamic parameters, namely potential temperature and wind speed.

4.2.2 Comparison with CALIOP L2 Aerosol Layer product

400 During the measurement period, 24 CALIPSO overpasses were available inside 1° radius around Gual
Pahari station. In 17 cases the boundary top location algorithm (SIBYL, Selective Iterated Boundary
Locator) identified two to four layers, whilst in 7 cases no layers were identified. For the 17 cases, the
PBL top from the ground-based lidar was available for 14 cases. In one case, the top of the second
layer was chosen, as the first one was inside the PBL, according to the attenuated backscatter image
405 from CALIOP. Furthermore, 5 cases were not included in the comparison as the detected layers were
either above the PBL (height >3 km) or in the free troposphere (height >10 km).

The final comparison of PBL heights between ground-based lidar FMI-Polly^{XT} and space-borne lidar
CALIOP was based on 9 cases and yielded an r of 0.84 (Figure 7). The slope (y - intercept set to zero)
was equal to 1.15, indicating that CALIPSO Layer Detection Algorithms probably detected aerosol
410 layers transported aloft the PBL, comprising mainly elevated smoke and dust layers, according to
aerosol subtype classification. These layers can blanket the PBL and cause strong attenuation of the
emitted laser beam. Thus, they can prohibit the detection of any underlying layer, which is likely to
correspond to the PBL top. Based on the analyzed cases, it was found that the overpass distance (here
20 and 101 km) from the lidar station and time difference between the measurements did not affect the
415 correlation of the PBL heights.

4.3 Statistical Analysis

4.3.1 PBL Diurnal Cycle

Figure 8a shows the mean diurnal PBL evolution as obtained by lidar measurements and ECMWF
estimations. Although night-time PBL height values were not taken into account for the statistical
420 analysis of PBL seasonal height, nocturnal values are included here so as to present the PBL diurnal
evolution.



According to the lidar measurements, the evolution of PBL began 2 to 4 h after sunrise with a daily PBL maximum of 1125 ± 88 m appearing, on average, at 10:00 UTC, approximately 3 h after the solar noon. The end of the growth period (90% of maximum height) appeared on average 1 h before the maximum PBL height was reached.

According to ECMWF model, a maximum PBL height of 1807 ± 805 m was reached at 09:00 UTC, with a time difference of 1h compared to FMI-Polly^{XT} observations. Moreover, the PBL evolution according to ECMWF estimations was stronger than the evolution given by FMI-Polly^{XT} data. This slight phase shift in PBL development can be attributed to the lower temporal resolution of ECMWF model compared to lidar measurements. ECMWF standard deviation values were lower during the early morning (00:00 and 03:00 UTC) and night-time period (15:00, 18:00 and 21:00 UTC), while during convective hours (06:00 and 09:00 UTC) they were significantly higher. During convective hours, the model overestimated PBL height, whereas during the night and early morning period it significantly underestimated PBL height. The latter, can be partly attributed to the fact that FMI-Polly^{XT} detects the RL top, while ECMWF estimates the nocturnal PBL top. The overall comparison between FMI-Polly^{XT} and ECMWF heights yielded an r of 0.86, whereas the mean normalized bias was quite large (58 %). In other words, FMI-Polly^{XT} and ECMWF top heights agreed well in terms of phase but magnitude discrepancies appeared.

In winter, the PBL cycle as defined by FMI-Polly^{XT} observations, reached a maximum height of 1028 ± 292 m at 11:00 UTC, while the CBL evolution was completed two hours earlier (Figure 8(b)). Standard deviation values of hourly PBL heights varied from 20 to 340 m, with the minimum values during the early morning period of 22:00-00:00 UTC and the maximum ones at 17:00 UTC.

According to ECMWF the maximum PBL height appeared at 09:00 UTC with a mean value of 2394 ± 932 m. The ECMWF overestimated PBL height during hours with strong convective activity (06:00, 09:00 and 12:00 UTC), whereas during night-time and early morning the PBL height was systematically underestimated. Higher standard deviation values appeared during convective hours, while lower standard deviation was found during night-time conditions. The overall comparison of PBL hourly heights from lidar and ECMWF revealed very satisfying agreement with an r of 0.9.

In the pre-monsoon period, the PBL diurnal cycle analyzed by FMI-Polly^{XT} data reached a maximum of 1249 ± 536 m at 12:00 UTC, with the PBL growth period completed three hours earlier (Figure 8(c)). Large standard deviation values were observed, especially between 07:00 and 12:00 UTC, a period which corresponds to the convective activity and the start of the PBL transition phase. Moreover, large standard deviation values persisted during the night-time period.

ECMWF estimations revealed a shorter but stronger PBL growth period, with a maximum top height of 2137 ± 143 m, which appeared earlier than the one given by FMI-Polly^{XT}. As in the annual and winter diurnal cycle, ECMWF overestimated PBL top height during convective hours. On the other hand, underestimation was observed during the early morning hours, with a more significant underestimation during night-time due to the fact that FMI-Polly^{XT} identified the RL, whereas the ECMWF estimated the nocturnal PBL top. The total comparison reached an r of 0.84.

In the monsoon season, the PBL daily evolution from FMI-Polly^{XT} data revealed a more or less steady PBL cycle (Figure 8(d)), with small diurnal fluctuations. A maximum PBL height of 1192 ± 187 m was



observed, on average, at 08:00 UTC, whilst the completion of the CBL growth occurred at 07:00 UTC, very close to the solar noon time. The highest standard deviation values were observed at 13:00-17:00 UTC.

465 The PBL development from ECMWF data revealed lower PBL heights than those retrieved from FMI-Polly^{XT}. The maximum height (889 ± 62 m) was reached at 09:00 UTC. The two methods showed better agreement during daytime, with an average relative difference of 27%. However, during night-time, ECMWF underestimated PBL height by 80% on average because the nocturnal PBL height was calculated contrary to the RL top that was identified by FMI-Polly^{XT}. The PBL diurnal cycle derived
470 from ECMWF was weaker compared to the cycle derived from FMI-Polly^{XT}. The total Pearson correlation coefficient was equal to 0.7.

4.3.2 Daily mean and maximum PBL height

In the following, we present the main statistical findings regarding the seasonal mean and maximum PBL cycle as observed from lidar measurements during 72 days. The seasonal cycle of mean and
475 maximum temperature is also examined. The seasonal mean PBL height was found at 695 ± 146 m during winter (17 days), 878 ± 297 m during the pre-monsoon period (15 days) and 1025 ± 296 m during the monsoon (40 days). Regarding the seasonal average maximum PBL height, it was found at 1191 ± 516 m during winter, 1326 ± 565 m during the pre-monsoon period and at 1361 ± 350 m during the monsoon. During the measurement days, a mean temperature of 21 ± 4 °C was found in the winter,
480 27 ± 3 °C in the pre-monsoon and 30 ± 2 °C in the monsoon season. A seasonal average maximum temperature of 29 ± 5 °C was recorded in the winter, 33 ± 4 °C in the pre-monsoon and 35 ± 2 °C in the monsoon period.

In general, the PBL seasonal cycle followed the temperature cycle of the measurement days very well. Furthermore, the temperature cycle observed during the measurement days was representative of the
485 seasonal temperature cycle of 2008-2009. In this sense, the seasonal cycle of PBL observed over Gual Pahari was weaker compared to the climatologically expected one. The smoother PBL cycle could be explained by maximum temperature anomaly. During winter, maximum temperature was on average 29 °C, a value 5 °C higher than the climatological one. On the other hand, during the pre-monsoon period, the average maximum temperature was 33 °C, which was 5 °C lower than the corresponding
490 climatological record. Thus, the relatively warmer winter and the comparatively colder pre-monsoon season jointly led to a rather indistinct PBL cycle in comparison to the one expected from long term climate statistics.

The highest inter-seasonal variability was exhibited during the pre-monsoon season both in terms of mean and maximum PBL height, which may be attributed to the meteorological conditions of this
495 period. During the pre-monsoon season, 7 cases with heavy rainfall (7-37 mm daily accumulated precipitation) and 8 cases with hardly any precipitation appeared (less than 3 mm accumulated precipitation). This combination led to a broad distribution of daily mean PBL heights (from 251 m to 1191 m). Large inter-seasonal variability was also observed in the winter period, in terms of maximum PBL height. The large standard deviation can be partly attributed to the broad inter-seasonal range of
500 maximum temperature, which was almost 16 °C (20 °C - 36 °C).



The frequency distribution of daily mean PBL height is presented in Figure 9 for 6 different classes of 300 m. During the measurement campaign, the majority of daily mean PBL heights were found between the classes of 600 and 1200 m (40% within 600-900 m; 32% within 900-1200 m). The winter period distribution was narrower and skewed towards the 600-900 m class. In the pre-monsoon and monsoon seasons, PBL height distributions were quite broader with a maximum between 900 and 1200 m. In terms of daily maximum PBL height, the majority of heights were found between 900 and 1800 m (26% within 900-1200 m; 22% within 1200-1500 m; 29% within 1500-1800 m). In the winter period, a more confined distribution appeared, with 53% of daily maximum heights between 900 and 1200 m. The PBL height spectrum was significantly broader in the pre-monsoon and monsoon periods, with maximum daily heights to spread between 600 and 1800 m.

4.3.3 PBL daily evolution rate

The distribution of daily growth rates is presented in Figure 9. For the whole measurement period, daily evolution rates were mostly observed in the 100-200 m/h class, while a significant number of mean growth rates was observed between 29-100 m/h. Different frequency distributions were observed on each seasonal period, albeit the average evolution rates did not exhibit strong seasonal variability. In the winter period, daily growth rates presented a slightly broad distribution with most of them lying between 100 and 200 m/h (40%), while a mean evolution rate of 157 ± 81 m/h ($N=15$) was found. In the pre-monsoon season, higher growth rates were observed, 206 ± 134 m/h ($N=9$), with 44% of them within the range 100-200 m/h, while 33% were between 200 and 300 m/h. Moreover, 11% of the daily growth rates lied in both classes 0-100 m/h and 500-600 m/h, supporting the high inter-seasonal variability that was found in Section 4.3.2 during the pre-monsoon season. In the monsoon season, lower evolution speeds were observed (121 ± 67 m/h, $N=22$), with 45% being less than 100 m/h., while a significant percentage (40%) was found between 100 and 200 m/h.

5 Comparison to another location

In this Section, the PBL characteristics in Gual Pahari are compared to the corresponding results from another location in South Africa, where the WCT method was also applied to lidar measurements. This site was located in similar surroundings and latitude (26° S) in Elandsfontein, South Africa (Korhonen et al., 2014).

The average PBL height was lower in Gual Pahari (866 m) in comparison to Elandsfontein (1400 m) with less seasonal variability (standard deviation of 165 m in Gual Pahari; 500 m in Elandsfontein). In both sites the maximum PBL height was reached approximately three hours after the solar noon, since the daily solar cycle is similar in the latitudes of the two stations. In Gual Pahari, the highest rates (mostly within 100-300 m/h) appeared in the pre-monsoon season (April-May), whilst in Elandsfontein maximum rates (between 120-320 m/h) were reached during spring (September-October). The pre-monsoon season in India and the spring season in South Africa have strong similarities.

6 Summary and Conclusions



In this paper, one year long ground-based lidar measurements were used to analyze PBL height variability over Gual Pahari, New Delhi. The lidar retrieved PBL heights were compared to data from independent sources; radiosondes, satellite observations and two atmospheric models. Three case studies of PBL daily evolution were discussed so as to identify atmospheric structures which can complicate PBL height detection. It was found, in support of previous work (Baars et al., 2008; Korhonen et al., 2013), that the modified WCT method performed well under different meteorological and aerosol load regimes. More specifically, a significantly good performance was revealed on a two day case, with multiple aerosol layers aloft. However, PBL determination was complicated before a rain event, where lofted layers created strong aerosol content gradients and later on, where diffuse aerosol layers appeared.

In the context of the aforementioned case studies, numerical estimations overestimated PBL height in the daytime, while an underestimation was observed in the night-time. The latter can be partly attributed to the fact that the lidar system identified the RL, whereas the numerical models estimated the nocturnal PBL top. The comparison between radiosonde and WRF vertical profiles, through three different methods, showed that radiosonde data overestimated PBL height in the night-time. The discrepancies between radiosonde and WRF PBL heights could be attributed to various sources, such as the different vertical resolution and the different nature of each data set; radiosondes provide in-situ measurements, whereas WRF model provides numerical estimations of various meteorological parameters. However, the fact that neither anthropogenic heat sources nor heat storage in buildings are included could also explain the model underestimation.

The comparison between lidar and radiosonde measurements performed well, especially during daytime. In the night-time, radiosonde profile data yielded lower PBL heights. There are several aspects behind the discrepancies of the two methods; namely, the distance between the lidar station and the radiosonde launch site, the different vertical resolution as well as the different approach followed for PBL height detection in each method. Additionally, during night-time, the lidar system detected the RL top, while radiosonde data identified the nocturnal PBL top. Detailed studies of the nocturnal boundary layer would require changes in the lidar configuration, employment of a near range and a far range telescope, which guarantees high quality PBL top detection even at heights lower than 100 m if this is a requirement (Baars et al., 2008).

CALIOP satellite observations correlated well with ground-based lidar data corroborating that the top of the first layer identified by CALIPSO Feature Detection Algorithms is a good estimation of the PBL top. This is in agreement with previous studies of Leventidou et al. (2013) and Korhonen et al. (2014). Space-borne lidar observations yielded, in general, higher PBL heights due to the detection of lofted aerosol layers in some of the cases.

The evolution of PBL started two to four hours after sunrise and was completed two hours after the solar noon, with the maximum PBL height observed approximately one hour later. In the winter and pre-monsoon season, ECMWF data revealed a stronger PBL daily evolution. During the monsoon season, both FMI-Polly^{XT} measurements and ECMWF output data, produced a smoother diurnal cycle, consisting of weaker fluctuations between daytime and night-time, with PBL heights from ECMWF



being systematically lower than those derived from FMI-Polly^{XT}. The latter can be attributed to the fact that FMI-Polly^{XT} detected the RL top, while ECMWF estimated the nocturnal PBL height.

The seasonal PBL cycle observed during the measurement campaign was less pronounced than the one expected from climatological records. This could be attributed to the combination of a relatively warmer winter and a colder pre-monsoon period with respect to long term climate statistics. The highest values of mean and maximum PBL height appeared in the monsoon season, where the highest mean and maximum temperature was recorded. The larger inter-seasonal variation in PBL height and daily PBL growth rate was observed in the pre-monsoon season, which was a transition period from the dry and relatively colder winter to the rainy and warmer monsoon period. During the measurement period, daily evolution rates of 29-200 m/h were mainly observed, with lower rates found on average in the rainy season of monsoon.

The PBL diurnal cycle and the mean daily PBL growth rates in Gual Pahari were very similar to those in Elandsfontein, a site with similar solar cycle and surroundings. Nevertheless, a lower average PBL height and a weaker seasonal variability were observed in Gual Pahari. The latter can be attributed to the frequent precipitation events which occurred in Gual Pahari especially during the late pre-monsoon and monsoon period.

In the future, the applicability of the modified WCT method can be tested in lidar systems with less operational cost, for instance to one-channel systems such as ceilometers and Doppler lidars. This would provide the potential of PBL determination on an operational basis.

595

Appendix. Statistical parameters formulas

Mean Normalized Bias

$$M_{NB} = \frac{1}{N} \sum_{i=1}^N \left(\frac{M_i - O_i}{O_i} \right) \times 100\%$$

Fractional Bias

600 $F_B = \frac{1}{N} \sum_{i=1}^N \left(\frac{M_i - O_i}{\frac{M_i + O_i}{2}} \right)$, range [-2,2], ideal value 0

Pearson Correlation Coefficient

$$R = \frac{\sum_{i=1}^N (O_i - \bar{O}) \cdot (M_i - \bar{M})}{\sqrt{\sum_{i=1}^N (O_i - \bar{O})^2} \cdot \sqrt{\sum_{i=1}^N (M_i - \bar{M})^2}}$$

M_i denotes predicted values from models, while O_i stands for observations at i , respectively. N is the number of samples.

605

Acknowledgements

This work (the campaigns) was partly funded by the European Integrated project on Aerosol Cloud Climate and Air Quality Interactions, EUCAARI. This work was supported by the Cy-Tera Project (NEA YPODOMH/STRATH/0308/31), which is co-funded by the European Regional Development Fund and the Republic of Cyprus through the Research Promotion Foundation.

610

References

Althausen, D., Engelmann, R., Baars, H., Heese, B., Ansmann, A., Müller, D., Komppula, M.: Portable Raman Lidar Polly^{XT} for Automated Profiling of Aerosol Backscatter, Extinction, and Depolarization.



- 615 Journal of Atmospheric and Oceanic Technology 26, 2366–2378.
<https://doi.org/10.1175/2009JTECHA1304.1>, 2009.
- Amiridis, V., Melas, D., Balis, D.S., Papayannis, A., Founda, D., Katragkou, E., Giannakaki, E., Mamouri, R.E., Gerasopoulos, E., Zerefos, C.: Aerosol Lidar observations and model calculations of the Planetary Boundary Layer evolution over Greece, during the March 2006 Total Solar Eclipse. Atmospheric Chemistry and Physics 7, 6181–6189, 2007.
- 620
- Baars, H., Ansmann, A., Engelmann, R., Althausen, D.: Continuous monitoring of the boundary-layer top with lidar. Atmospheric chemistry and Physics 8, 7281–7296, 2008.
- 625
- Beljaars, A. C. M.: The impact of some aspects of the boundary layer scheme in the ECMWF model. In Proc. of ECMWF Seminar on Parameterization of Sub-grid Scale Physical Processes, pp. 125{161, Reading, 5{9 September 1994, 1995.
- 630
- Beljaars, A. C. M. and Viterbo, P.: The role of the boundary layer in a numerical weather prediction model. In A. A. M. Holtslag and P. G. Duynkerke (Eds), Clear and Cloudy Boundary Layers, North Holland Publishers, 1999.
- Boers, R., Eloranta, E.W.: Lidar measurements of the atmospheric entrainment zone and the potential temperature jump across the top of the mixed layer. Boundary-Layer Meteorology 34, 357–375, 1986.
- 635
- Bravo-Aranda, J. A., de Arruda-Moreira, G., Navas-Guzmán, F., Granados-Muñoz, M. J., Guerrero-Rascado, J. L., Pozo-Vázquez, D., Arbizu-Barrena, C., Olmo, F. J., Mallet, M., and Alados-Arboledas, L.: PBL height estimation based on lidar depolarisation measurements (POLARIS), Atmospheric Chemistry and Physics Discussions, 2016, 1–24, <https://doi.org/10.5194/acp-2016-718>, 2016.
- 640
- Brooks, I.M.: Finding boundary layer top: Application of a wavelet covariance transform to lidar backscatter profiles. Journal of Atmospheric and Oceanic Technology 20, 1092–1105, 2003.
- 645
- Chen, F., Dudhia, J.: Coupling an advanced land surface–hydrology model with the Penn State–NCAR MM5 modeling system. Part I: Model implementation and sensitivity. Monthly Weather Review 129, 569–585, 2001.
- 650
- Cimini, D., De Angelis, F., Dupont, J.-C., Pal, S., Haeffelin, M.: Mixing layer height retrievals by multichannel microwave radiometer observations. Atmospheric Measurement Techniques 6, 2941–2951. <https://doi.org/10.5194/amt-6-2941-2013>, 2013.
- Cohn, S. A. and Angevine, W. M.: Boundary layer height and entrainment zone thickness measured by lidars and wind-profiling radars, J. Appl. Meteorol., 39, 1233–1247, 2000.
- 655
- Davis, K.J., Gamage, N., Hagelberg, C.R., Kiemle, C., Lenschow, D.H., Sullivan, P.P.: An objective method for deriving atmospheric structure from airborne lidar observations. Journal of Atmospheric and Oceanic Technology 17, 1455–1468, 2000.
- 660
- de Arruda Moreira, G. and Guerrero-Rascado, J. L. and Benavent-Oltra, J. A. and Ortiz-Amezcuca, P. and Román, R. and Esteban Bedoya-Velázquez, A. and Bravo-Aranda, J. A. and Olmo-Reyes, F. J. and Landulfo, E. and Alados-Arboledas, L.: Analyzing the turbulence in the Planetary Boundary Layer by the synergic use of remote sensing systems: Doppler wind lidar and aerosol elastic lidar. Atmospheric Chemistry and Physics Discussions, 1-24, 10.5194/acp-2018-276, 2018.
- 665
- Dudhia J.: Numerical Study of Convection Observed during the Winter Monsoon Experiment Using a Mesoscale Two-Dimensional Model, J. Atmos. Sci., 46, 3077-3107, 1989.
- 670
- ECMWF: IFS Documentation – Cy36r1, part 5: Ensemble prediction system, ECMWF, 2010a.
ECMWF: IFS Documentation – Cy36r1, part 4: Physical processes, ECMWF, 2010b.
ECMWF: IFS Documentation – Cy36r1, ECMWF, 2010c.
- Emeis, S., Munkel, C., Vogt, S., Müller, W. and Schafer, K.: Atmospheric boundary-layer structure from simultaneous SODAR, RASS, and ceilometer measurements, Atmos. Environ., 38, 273–286, 2004.



- 675 Engelmann, R., Wandinger, U., Ansmann, A., Müller, D., Zeromskis, E., Althausen, D., and Wehner, B.: Lidar observations of the vertical aerosol flux in the planetary boundary layer, *J. Atmos. Ocean. Tech.*, 25, 1296–1306, 2008.
- 680 Engelmann, R. and Kanitz, T. and Baars, H. and Heese, B. and Althausen, D. and Skupin, A. and Wandinger, U. and Komppula, M. and Stachlewska, I. S. and Amiridis, V. and Marinou, E. and Mattis, I. and Linn, H. and Ansmann, A.: The automated multiwavelength Raman polarization and water-vapor lidar Polly^{XT}: the neXT generation. *Atmospheric Measurement Techniques*. 4, 1767–1784 [10.5194/amt-9-1767-2016](https://doi.org/10.5194/amt-9-1767-2016), 2016.
- 685 Garratt, J. R.: *The Atmospheric Boundary Layer*, 335 pp., Cambridge Atmospheric and Space Science Series, Cambridge Univ. Press, 1992.
- 690 Groß, S., Gasteiger, J., Freudenthaler, V., Wiegner, M., Geiß, A., Schladitz, A., Toledano, C., Kandler, K., Tesche, M., Ansmann, A. and Wiedensohler, A.: Characterization of the planetary boundary layer during SAMUM-2 by means of lidar measurements. *Tellus* 63B, 695–705, [doi:10.1111/j.1600-0889.2011.00557.x](https://doi.org/10.1111/j.1600-0889.2011.00557.x), 2011.
- 695 Haeffelin, M., Angelini, F., Morille, Y., Martucci, G., Frey, S., Gobbi, G.P., Lolli, S., O’Dowd, C.D., Sauvage, L., Xueref-Rémy, I., Wastine, B., Feist, D.G.: Evaluation of Mixing-Height Retrievals from Automatic Profiling Lidars and Ceilometers in View of Future Integrated Networks in Europe. *Boundary-Layer Meteorology* 143, 49–75. <https://doi.org/10.1007/s10546-011-9643-z>, 2012.
- 700 Hegde, P., Pant, P., Naja, M., Dumka, U. C., and Sagar, R.: South Asian dust episode in June 2006: Aerosol observations in the central Himalayas, *Geophys. Res. Lett.*, 34, L23802, [doi:10.1029/2007GL030692](https://doi.org/10.1029/2007GL030692), 2007.
- Hong, S.-Y., Noh, Y., Dudhia, J.: A new vertical diffusion package with an explicit treatment of entrainment processes. *Monthly weather review* 134, 2318–2341, 2006.
- 705 Hong, S.-Y., Kim, S.-W.: Stable boundary layer mixing in a vertical diffusion scheme. Proc. Ninth Annual WRF User’s Workshop, Boulder, CO, National Center for Atmospheric Research, 3.3. [Available online at <http://www.mmm.ucar.edu/wrf/users/workshops/WS2008/abstracts/3-03.pdf>], 2008
- 710 Hyvärinen, A.-P., Lihavainen, H., Komppula, M., Panwar, T.S., Sharma, V.P., Hooda, R.K., Viisanen, Y.: Aerosol measurements at the Gual Pahari EUCAARI station: preliminary results from in-situ measurements. *Atmospheric Chemistry and Physics* 10, 7241–7252, 2010.
- 715 Hyvärinen, A.-P., Raatikainen, T., Komppula, M., Mielonen, T., Sundström, A.-M., Brus, D., Panwar, T.S., Hooda, R.K., Sharma, V.P., de Leeuw, G., Lihavainen, H.: Effect of the summer monsoon on aerosols at two measurement stations in Northern India – Part 2: Physical and optical properties. *Atmospheric Chemistry and Physics* 11, 8283–8294. <https://doi.org/10.5194/acp-11-8283-2011>, 2011.
- 720 Jiménez, P.A., Dudhia, J., González-Rouco, J.F., Navarro, J., Montávez, J.P., García-Bustamante, E.: A Revised Scheme for the WRF Surface Layer Formulation. *Monthly Weather Review* 140, 898–918. <https://doi.org/10.1175/MWR-D-11-00056.1>, 2012.
- 725 Jordan, N.S., Hoff, R.M., Bacmeister, J.T.: Validation of Goddard Earth Observing System-version 5 MERRA planetary boundary layer heights using CALIPSO: VALIDATION OF GEOS-5 USING CALIPSO. *Journal of Geophysical Research: Atmospheres* 115. <https://doi.org/10.1029/2009JD013777>, 2010.
- Kain, J. S. and Fritsch, J. M.: A one-dimensional entraining/ detraining plume model and its application in convective parameterization, *J. Atmos. Sci.*, 47, 2784–2802, 1990.
- 730 Kain, J. S. and Fritsch, J. M.: Convective parameterization for mesoscale models: The Kain-Fritsch scheme. The representation of cumulus convection in numerical models, K. A. Emanuel and D.J. Raymond, Eds., *Amer. Meteor. Soc.*, 246 pp, 1993.



- 735 Komppula, M., Mielonen, T., Arola, A., Korhonen, K., Lihavainen, H., Hyvärinen, A.-P., Baars, H., Engelmann, R., Althausen, D., Ansmann, A., Müller, D., Panwar, T.S., Hooda, R.K., Sharma, V.P., Kerminen, V.-M., Lehtinen, K.E.J., Viisanen, Y.: Technical Note: One year of Raman-lidar measurements in Gual Pahari EUCAARI site close to New Delhi in India – Seasonal characteristics of the aerosol vertical structure. *Atmospheric Chemistry and Physics* 12, 4513–4524. <https://doi.org/10.5194/acp-12-4513-2012>, 2012.
- 740 Korhonen, K., Giannakaki, E., Mielonen, T., Pfüller, A., Laakso, L., Vakkari, V., Baars, H., Engelmann, R., Beukes, J.P., Van Zyl, P.G., Ramandh, A., Ntsangwane, L., Josipovic, M., Tiitta, P., Fourie, G., Ngwana, I., Chiloane, K., Komppula, M.: Atmospheric boundary layer top height in South Africa: measurements with lidar and radiosonde compared to three atmospheric models. *Atmospheric Chemistry and Physics* 14, 4263–4278. <https://doi.org/10.5194/acp-14-4263-2014>, 2014.
- 745 Kulmala, M., Asmi, A., Lappalainen, H. K., Baltensperger, U., Brenguier, J.-L., Facchini, M. C., Hansson, H.-C., Hov, Ø., O’Dowd, C. D., P’oschl, U., Wiedensohler, A., Boers, R., Boucher, O., de Leeuw, G., Denier van den Gon, H., Feichter, J., Krejci, R., Laj, P., Lihavainen, H., Lohmann, U., McFiggans, G., Mentel, T., Pilinis, C., Riipinen, I., Schulz, M., Stohl, A., Swietlicki, E., Vignati, E., Amann, M., Ammann, M., General overview: European Integrated project on Aerosol Cloud Climate and Air Quality interactions (EUCAARI) – integrating aerosol research from nano to global scales. *Atmos. Chem. Phys.*, 11, 13061–13143, doi:10.5194/acp-11-13061-2011, 2011.
- 750 Lammert, A., Bösenberg, J.: Determination of the convective boundary-layer height with laser remote sensing. *Boundary-Layer Meteorology* 119, 159–170. <https://doi.org/10.1007/s10546-005-9020-x>, 2006.
- 755 Lange, D., et al., 2014: Atmospheric boundary layer height monitoring using a Kalman filter and backscatter lidar returns, *IEEE Transactions on Geos. Rem. Sensing*, **52**, 4717-4728, doi:10.1109/TGRS.2013.2284110.
- 760 Lau W.K.M., Kim K.M., Hsu C.N. Possible influences of air pollution, dust- and sandstorms on the Indian monsoon. *WMO Bulletin* 58 (1)-January 2009. Lelieveld, J., Crutzen, P. J., Ramanathan, V., Andreae, M. O., Brenninkmeijer, C. A. M., Campos, T., Cass, G. R., Dickerson, R. R., Fischer, H., de Gouw, J. A., Hansel, A., Jefferson, A., Kley, D., de Laat, A. T. J., Lal, S., Lawrence, M. G., Lobert, J. M., Mayol-Bracero, O. L., Mitra, A. P., Novakov, T., Oltmans, S. J., Prather, K. A., Reiner, T., Rodhe, H., Scheeren, H. A., Sikka, D., and Williams, J.: The Indian Ocean Experiment: Widespread air pollution from South and Southeast Asia, *Science*, 291, 1031–1036, 2001.
- 765 Leventidou, E., Zanis, P., Balis, D., Giannakaki, E., Pytharoulis, I., Amiridis, V.: Factors affecting the comparisons of planetary boundary layer height retrievals from CALIPSO, ECMWF and radiosondes over Thessaloniki, Greece. *Atmospheric environment* 74, 360–366., 2013.
- 770 Louis, J. F., Tiedtke, M. and Geleyn, J.-F. (1982). A short history of the operational PBL parametrization at ECMWF. In Proc. ECMWF Workshop on Boundary Layer Parametrization, pp. 59{80, Reading, 25{27 November 1981.
- 775 McGrath-Spangler, E. L. and Denning, A. S.: Estimates of North American Summertime Planetary Boundary Layer Depths Derived from Space-borne Lidar, *J. Geophys. Res.*, 117, D15101, doi:10.1029/2012JD017615, 2012.
- 780 Melfi, S.H., Spinhirne, J.D., Chou, S.H., Palm, S.P.: Lidar observation of the vertically organized convection in the planetary boundary layer over the ocean. *J. Clim. Appl. Meteorol.* 24, 806e821, 1985.
- Menut, L., Flamant, C., Pelon, J. and Flamant, P. H.: Urban boundary-layer height determination from lidar measurements over the Paris area, *Appl. Opt.*, 38, 945–954, 1999.
- 785 Mlawer E. J., Taubman S. J., Brown P. D., Iacono M. J. and Clough S. A.: Radiative transfer for inhomogeneous atmospheres: RRTM, a validated correlated-k model for the longwave, *J. Geophys. Res.*, 102 (D14), 16663-16682, 1997.



- 790 Morille, Y., Haeffelin, M., Drobinski, P., and Pelon, J.: STRAT: an automated algorithm to retrieve the vertical structure of the atmosphere from single-channel lidar data, *J. Atmos. Ocean. Tech.*, 24, 761–775, 2007.
- 795 Nakajima, T., Yoon, S.-C., Ramanathan, V., Shi, G.-Y., Takemura, T., Higurashi, A., Takamura, T., Aoki, K., Sohn, B. J., Kim, S.-W., Tsuruta, H., Sugimoto, N., Shimizu, A., Tanimoto, H., Sawa, Y., Lin, N.-H., Lee, C.-T., Goto, D., and Schutgens, N.: Overview of the atmospheric Brown Cloud East Asian Regional Experiment 2005 and a study of the aerosol direct radiative forcing in east Asia, *J. Geophys. Res.*, 112, D24S91, doi:10.1029/2007JD009009, 2007.
- 800 Nieuwstadt, F. T. M.: The turbulent structure of the stable, nocturnal boundary layer. *J. Atmos. Sci.*, 41, 2202–2216, 1984.
- 805 Oke, T. R.: *Boundary Layer Climates*, 2nd ed., 435 pp., Halsted Press, New York, 1988.
Palm, S. P., Hagan, D., Schwemmer, G., Melfi, S. H.: Inference of marine atmospheric boundary layer moisture and temperature structure using airborne lidar and infrared radiometer data. *J. Appl. Meteorol.* 37, 308e324. CrossRef, Web of Science_ Times Cited: 7, ADS, 1998.
- 810 Palm, S. P., Benedetti, A., Spinhirne, J.: Validation of ECMWF global forecast model parameters using GLAS atmospheric channel measurements. *Geophys. Res. Lett.* 32, 2005.
- 815 Perrino, C., Tiwari, S., Catrambone, M., Torre, D. D., Rantica, E., Canepari, S.: Chemical characterization of atmospheric PM in Delhi, India, during different periods of the year, including Diwali festival. *Atmos Pollut. Res.* 2, 418–427, 2011.
- 820 Pielke, R. A., Davey, C. A., Niyogi, D., Fall, S., Steinweg-Woods, J., Hubbard, K., Lin, X., Cai, M., Lim, Y. K., and Li, H.: Unresolved issues with the assessment of multidecadal global land surface temperature trends, *J. Geophys. Res.*, 112, D16113, doi:10.1029/2006JD008229, 2007.
- 825 Ramanathan, V., Li, F., Ramana, M. V., Praveen, P. S., Kim, D., Corrigan, C. E., Nguyen, H., Stone, E. A., Schauer, J. J., Carmichael, G. R., Adhikary, B., and Yoon, S. C.: Atmospheric brown clouds: Hemispherical and regional variations in longrange transport, absorption, and radiative forcing, *J. Geophys. Res.*, 112, D22S21, doi:10.1029/2006JD008124, 2007a.
- 830 Reddy, M. S. and Venkataraman, C.: Inventory of aerosol and sulphur dioxide emissions from India: I—Fossil fuel combustion, *Atmos. Environ.*, 36, 677–697, 2002a.
- 835 Reddy, M. S. and Venkataraman, C.: Inventory of aerosol and sulphur dioxide emissions from India. Part II—biomass combustion, *Atmos. Environ.*, 36, 699–712, 2002b.
- 840 Scarino, A. J., Obland, M. D., Fast, J. D., Burton, S. P., Ferrare, R. A., Hostetler, C. A., Berg, L. K., Lefer, B., Haman, C., Hair, J. W., Rogers, R. R., Butler, C., Cook, A. L. and Harper, D. B.: Comparison of mixed layer heights from airborne high spectral resolution lidar, ground-based measurements, and the WRF-Chem model during CalNex and CARES, *Atmos. Chem. Phys. Discuss.*, 13, 13721–13772, doi:10.5194/acpd-13-13721-2013, 2013.
- 845 Seibert, P., Beyrich, F., Gryning, S. E., Joffre, S., Rasmussen, A. and Tercier, Ph.: Review and intercomparison of operational methods for the determination of the mixing height, *Atmos.*, 34, 1001–1027, 2000.
- 850 Seidel, D. J., Ao, C. O., Li, K.: Estimating climatological planetary boundary layer heights from radiosonde observations: Comparison of methods and uncertainty analysis. *Journal of Geophysical Research* 115. <https://doi.org/10.1029/2009JD013680>, 2010.
- 855 Shin, H. H. and Hong, S.-Y.: Intercomparison of planetary boundary-layer parameterizations in the WRF model for a single day from CASES-99. *Boundary-Layer Meteorol.* 139, 261–281, 2011.
- 860 Skamarock, W. C., Klemp, J. B., Dudhia, J., Gill, D. O., Barker, D. M., Wang, W., Powers, J. G.: A description of the advanced research WRF version 2. National Center For Atmospheric Research Boulder Co Mesoscale and Microscale Meteorology Div, 2005.



- 850 Sorbjan, Z.: Structure of the Atmospheric Boundary Layer, 317 pp., Prentice Hall, Englewood Cliffs, N.J., 1989.
- Stull, R. B.: An Introduction to Boundary Layer Meteorology, 666 pp., Dordrecht, Kluwer, 1988.
- Summa, D., Di Girolamo, P., Stelitano, D. and Cacciani, M.: Characterization of the planetary boundary layer height and structure by Raman lidar: comparison of different approaches, Atmos. Meas. Tech. Discuss., 6, 5195-5216, doi:10.5194/amt-d-6-5195-2013, 2013.
- 855 Thompson, G., Field, P.R., Rasmussen, R.M., Hall, W.D.: Explicit Forecasts of Winter Precipitation Using an Improved Bulk Microphysics Scheme. Part II: Implementation of a New Snow Parameterization. Monthly Weather Review 136, 5095–5115. <https://doi.org/10.1175/2008MWR2387.1>, 2008.
- 860 Tsaknakis, G., Papayannis, A., Kokkalis, P., Amiridis, V., Kambezidis, H.D., Mamouri, R.E., Georgoussis, G., Avdikos, G.: Inter-comparison of lidar and ceilometer retrievals for aerosol and Planetary Boundary Layer profiling over Athens, Greece. Atmospheric Measurement Techniques 4, 1261–1273. <https://doi.org/10.5194/amt-4-1261-2011>, 2011.
- 865 Vaughan, M.A., Young, S.A., Winker, D.M., Powell, K.A., Omar, A.H., Liu, Z., Hu, Y., Hostetler, C.A.: Fully automated analysis of space-based lidar data: an overview of the CALIPSO retrieval algorithms and data products, in: Singh, U.N. (Ed.), . p. 16. <https://doi.org/10.1117/12.572024>, 2004.
- 870 Vickers, D., L. Mahrt, L.: The cospectral gap and turbulent flux calculations. J. Atmos. Oceanic Technol., 20, 627–660, 2003.
- Viterbo, P., Beljaars, A. C. M., Mahouf, J.-F. and Teixeira, J: The representation of soil moisture freezing and its impact on the stable boundary layer. Q. J. R. Meteorol. Soc., 125, 2401-2426, 1999.
- 875 Vogelesang, Holtslag: Evaluation and modern impacts of alternative boundary-layer height formulations. Bound. Layer Meteor. 81, 245-269, 1996.
- Wang, K. C., Dickinson, R. E., and Shunlin, L.: Clear sky visibility has decreased over land globally from 1973 to 2007, Science, 323, 1468–1470, doi:10.1126/science.1167549, 2009.
- 880 Wang, X.Y., Wang, K.C.: Estimation of atmospheric mixing layer height from radiosonde data. Atmospheric Measurement Techniques 7, 1701–1709. <https://doi.org/10.5194/amt-7-1701-2014>, 2014.
- Winker, D.H.: CALIOP Algorithm Theoretical Basis. In: CALIOP Instrument, and Algorithms Overview. NASA, 2006.
- 885 Zilitinkevich, Sergej, Baklanov, Alexander: Calculation of the Height of Stable Boundary Layers in Operational Models. Danish Meteorological Institute, Copenhagen, 2001.
- 890



Table 1: The data sources used in this study, spatiotemporal resolution and the corresponding PBL determination method.

Method	Temporal resolution	Vertical resolution	Horizontal resolution	PBL height determination
Raman lidar FMI-Polly ^{XT}	15min averages of 30sec scans	30m	point measurement	maximum mixing height via aerosol layer top height
CALIOP aboard CALIPSO	16-day repeat cycle	30m	5km	Feature Detection and Layer Properties Algorithm
Radiosondes	12 h	minimum 50 m	point measurement	BRN (Ricr=0.21)
ECMWF	3h	62 pressure levels	1.0° (≈ 100km)	BRN (Ricr=0.25)
WRF	1h	37 Eta-levels up to 50hPa	0.02° (≈ 2km)	BRN (Ricr=0.25 over land)

895

900

905

910

915



Table 2: Night-time (00:00 UTC), except for 12 February 2009 (3:00 UTC) PBL top height calculated through T_{crit} , RH_{crit} and θ_{crit} methods, applied to WRF and radiosonde profile data.

	T_{crit}		θ_{crit}		RH_{crit}	
	PBL height (m AGL)		PBL height (m AGL)		PBL height (m AGL)	
	<i>WRF</i>	<i>radiosonde</i>	<i>WRF</i>	<i>radiosonde</i>	<i>WRF</i>	<i>radiosonde</i>
12-Feb-09	172	-	131	435	131	435
01-Mar-09	171	-	171	-	130	-
02-Mar-09	78	225	78	225	78	225
29-Jun-08	913	-	913	833	913	833

925

930

935

940

945

950



Table 3: As in Table 2, but for daytime (12:00 UTC).

	T_crit PBL height (m AGL)		θ_crit PBL height (m AGL)		RH_crit PBL height (m AGL)	
	<i>WRF</i>	<i>radiosonde</i>	<i>WRF</i>	<i>radiosonde</i>	<i>WRF</i>	<i>radiosonde</i>
12-Feb-09	1425	1387	1425	1387	1213	1069
01-Mar-09	-	-	716	582	716	582
02-Mar-09	-	-	906	-	906	544
29-Jun-08	-	-	1490	1490	1490	1490

955

960

965

970

975

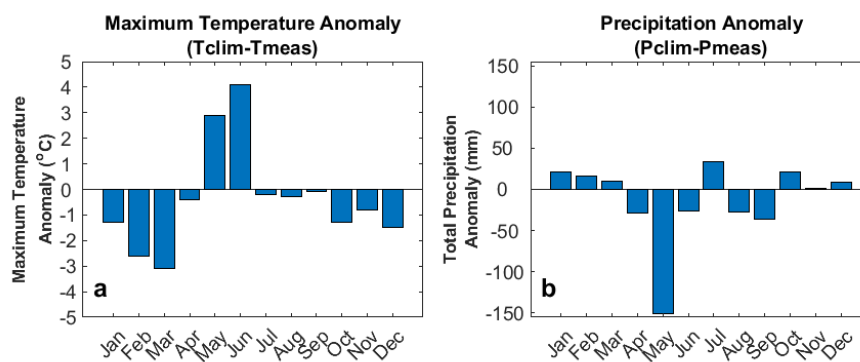


Figure 1: Maximum temperature and total precipitation anomaly at New Delhi on a monthly basis. The bars indicate the difference between the climatological values and the corresponding values during the measurement campaign.

980

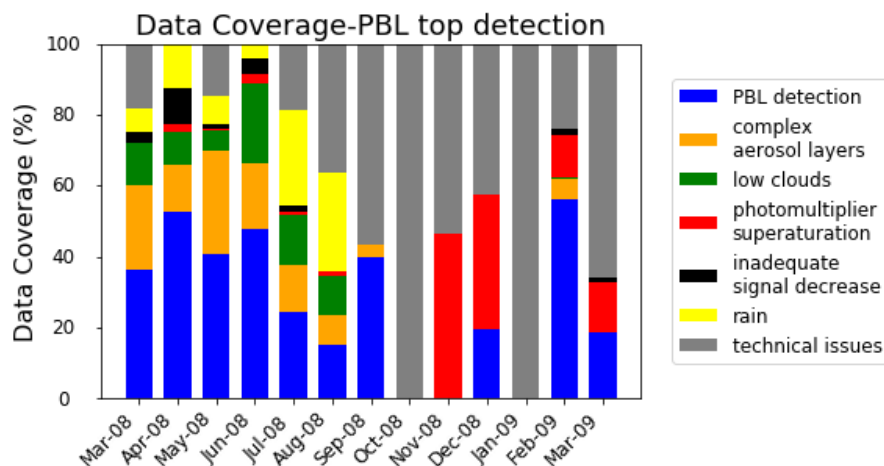
985

990

995

1000

1005



1010 **Figure 2:** Data coverage of lidar measurements during March 2008-March 2009 classified into seven
 different categories. Coverage is calculated with respect to total convective hours (from 4 h after
 sunrise to 1 h before sunset) during the measurement days of the campaign.

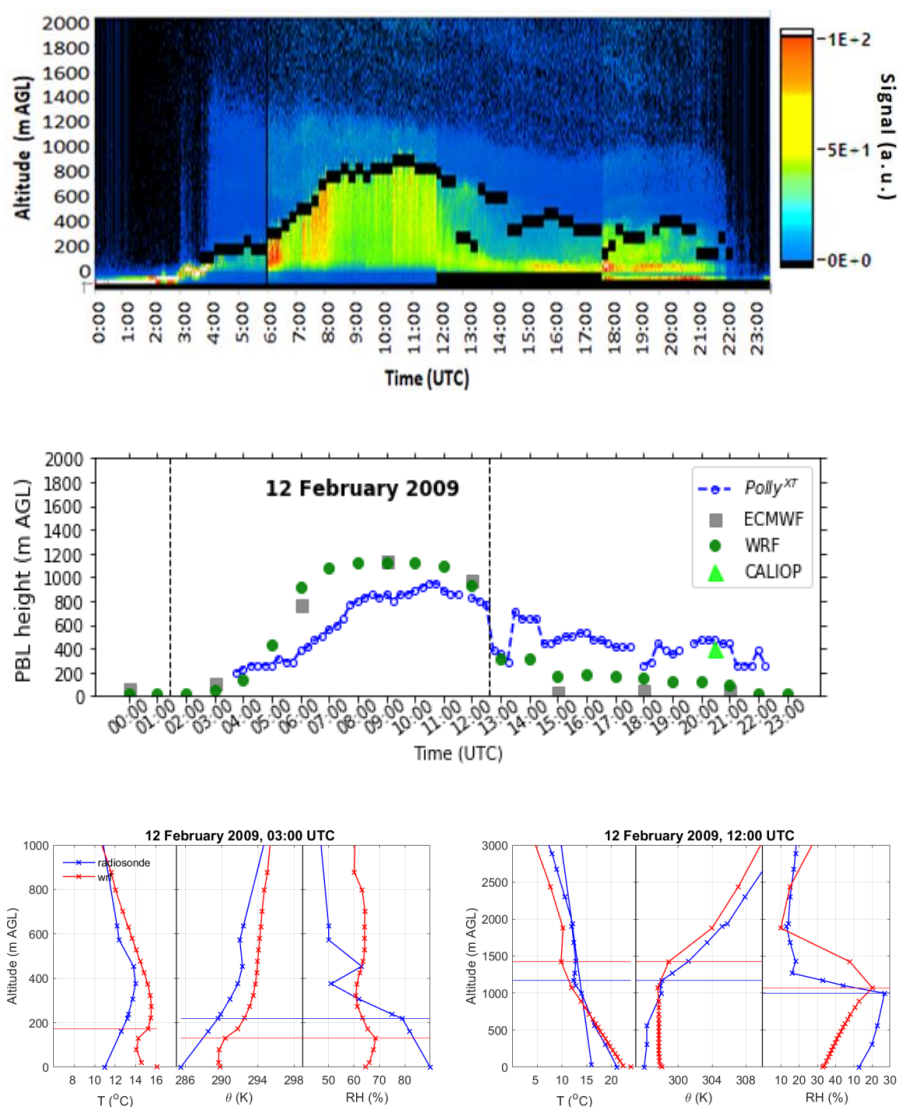
1015

1020

1025

1030

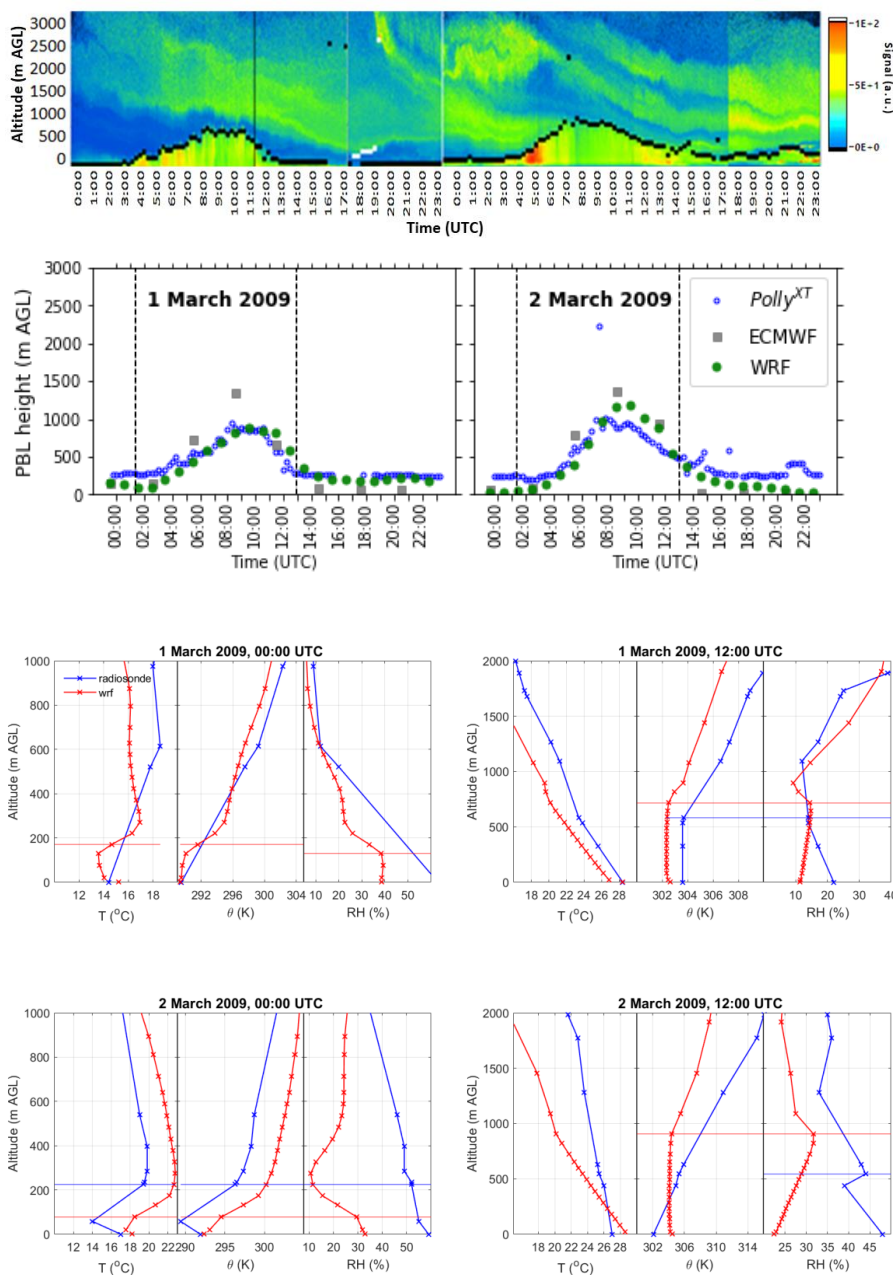
1035



1040

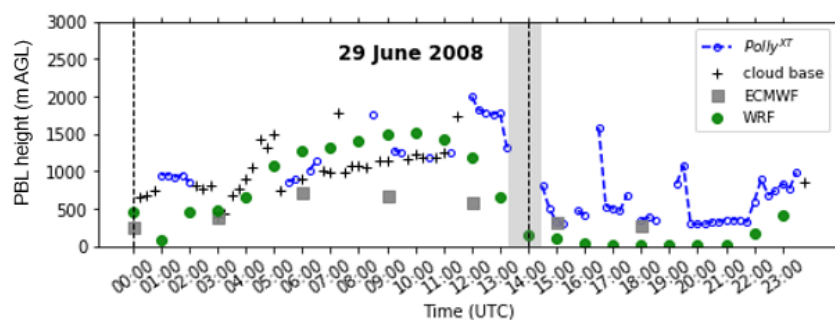
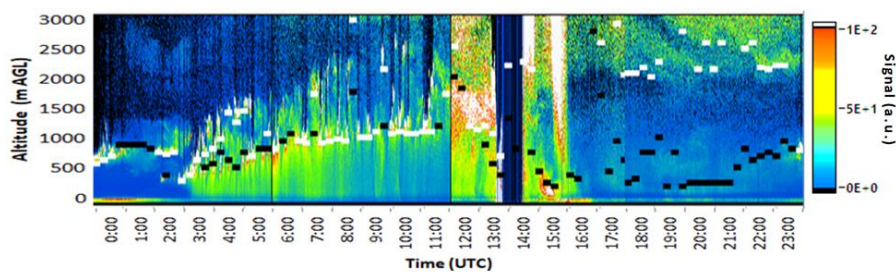
Figure 3: Evolution of PBL height observed on 12 February 2009. Range-corrected signal (top) at 1064 nm as measured with FMI-Polly^{XT} (black lines indicate 15 min values of PBL height). PBL height (middle) as given by the FMI-Polly^{XT}, ECMWF, WRF and CALIOP (vertical lines indicate sunrise and sunset times). Vertical profiles of T, θ and RH (bottom) as determined by WRF model and radiosonde data (horizontal lines show the PBL height).

1045



1050

Figure 4: Same as Fig. 3 except for 1-2 March 2009. White horizontal lines (top) indicate 15 min values of cloud base height.



1055

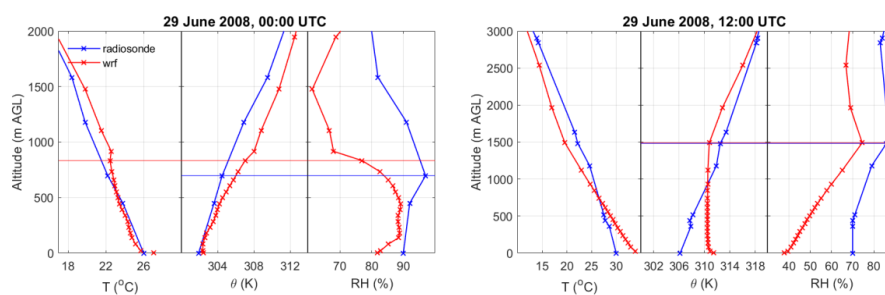
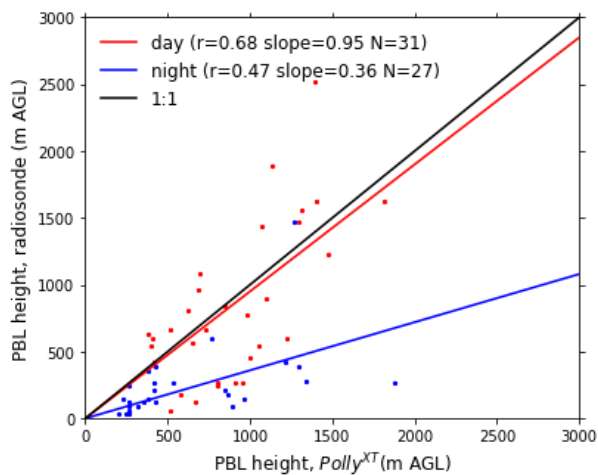


Figure 5: Same as Fig. 3 except for 29 June 2008. White horizontal lines (top) indicate 15 min values of cloud base height. Grey shading (middle) indicates rainfall.

1060



1065

Figure 6: Scatter plots for comparison of FMI-Polly^{XT} to daytime (12:00 UTC) and night-time (00:00 UTC) radiosonde observations throughout the measurement campaign.

1070

1075

1080

1085

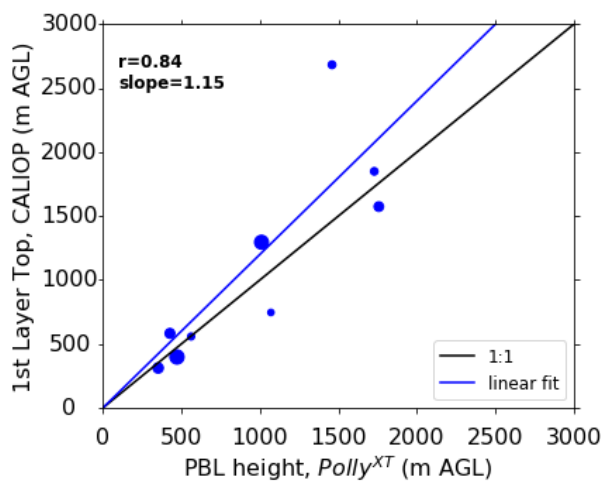


Figure 7: PBL top height comparison of 9 common cases for FMI-Polly^{XT} and CALIOP data. The heights given by CALIOP have been corrected with elevation. The markersize is proportional to the overpass distance from the ground-based lidar, with a range of 20-101 km.

1090

1095

1100

1105

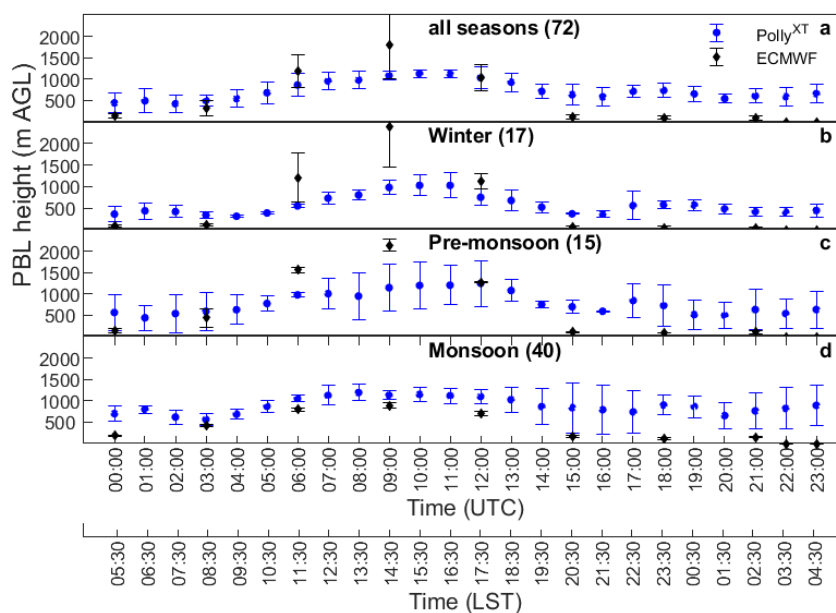


Figure 8: PBL average diurnal cycle in Gual Pahari according to FMI-Polly^{XT} and ECMWF estimations during March 2008-March 2009 (a), Winter (b), Pre-monsoon (c) and Monsoon season (d). Numbers indicate data availability for each independent source.

1115

1120

1125

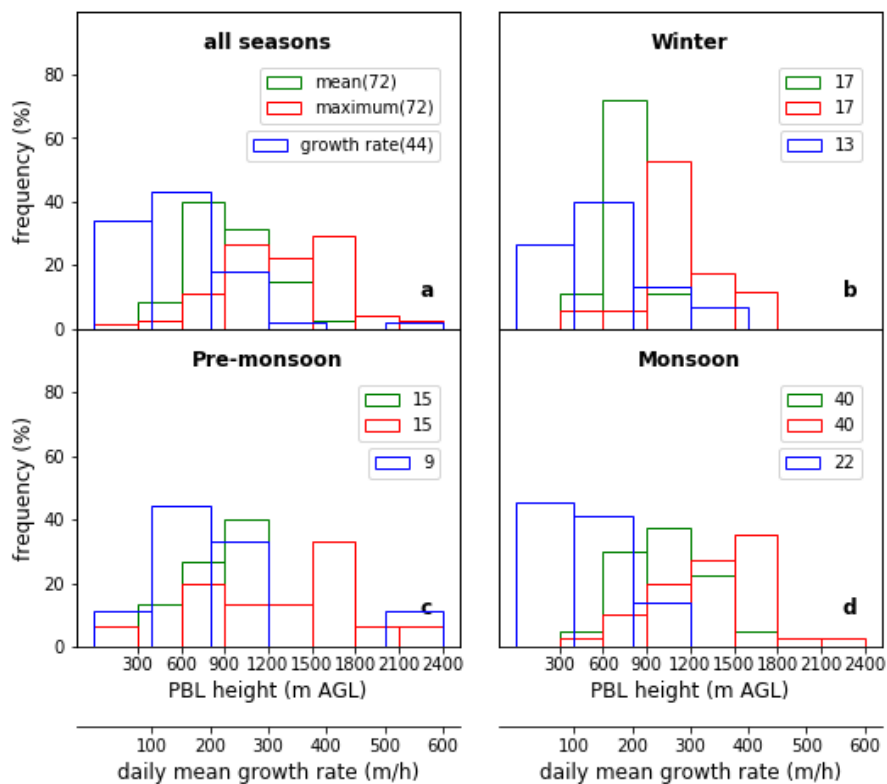


Figure 9: Frequency distribution of daily mean and maximum PBL height as calculated throughout the measurement period (a), the winter period (b), the pre-monsoon season (c) and the monsoon period (d).

1130 Numbers indicate data availability.